

Accurate retrieval of structural information from laser-induced photoelectron and high-harmonic spectra by few-cycle laser pulses

Toru Morishita,^{1,2} Anh-Thu Le,¹ Zhangjin Chen¹ and C. D. Lin¹

¹*Department of Physics, Cardwell Hall, Kansas State University, Manhattan, KS 66506, USA*

²*Department of Applied Physics and Chemistry, University of Electro-Communications,
1-5-1 Chofu-ga-oka, Chofu-shi, Tokyo, 182-8585, Japan*

(Dated: February 8, 2022)

By analyzing “exact” theoretical results from solving the time-dependent Schrödinger equation of atoms in few-cycle laser pulses, we established the general conclusion that differential elastic scattering and photo-recombination cross sections of the target ion with *free* electrons can be extracted accurately from laser-generated high-energy electron momentum spectra and high-order harmonic spectra, respectively. Since both electron scattering and photoionization (the inverse of photo-recombination) are the conventional means for interrogating the structure of atoms and molecules, this result shows that existing few-cycle infrared lasers can be implemented for ultrafast imaging of transient molecules with temporal resolution of a few femtoseconds.

PACS numbers: 42.65.Ky, 33.80.Rv

Electron diffraction and X-ray diffraction are the conventional methods for imaging molecules to achieve spatial resolution of better than sub-Angstroms, but they are incapable of achieving temporal resolutions of femto- to tens of femtoseconds, in order to follow chemical and biological transformations. To image such transient events, large facilities like ultrafast electron diffraction method [1] and X-ray free-electron lasers (XFELs) are being developed. Instead of pursuing these expensive technologies, here we provide the needed quantitative analysis to show that existing few-cycle infrared lasers can be implemented for ultrafast imaging of transient molecules.

When an atom is exposed to an infrared laser, the atom is first tunnel ionized with the release of an electron. This electron is placed in the oscillating electric field of the laser and may be driven back to revisit its parent ion. This re-encounter incurs, in the second step, various elastic and inelastic electron-ion collision phenomena where the structural information of the target is embedded. The possibility of using such laser-induced returning electrons for self-imaging molecules has been discussed frequently in the past. Theoretical studies of laser-induced electron momentum images of simple molecules do show interference maxima and minima typical of diffraction images, but they are observed only for large internuclear distances [2, 3, 4, 5, 6]. In addition, for quantitative analysis, the role of laser fields on these diffraction images still has to be understood [3]. More recently, it was reported that the outermost molecular orbital of N₂ molecules can be extracted from the high-harmonic generation (HHG) spectra using the tomographic procedure [7]. This interesting result has generated a lot of excitement, but the reported results are obtained based on a number of assumptions [8, 9, 10]. To make dynamic chemical imaging with infrared lasers as a practical tool, general theoretical considerations, especially the validity of the extraction procedure, should be examined carefully.

In this Letter, we show that elastic scattering cross sections of the target ion by free electrons can be accurately extracted from laser-induced photoelectron momentum spectra. We also show that accurate photo-recombination cross sections of the target ion can be extracted from the HHG spectra. Our conclusions are based on “exact” theoretical results by solving the time-dependent Schrödinger equations (TDSE) of several atoms in intense laser fields. While our conclusions are derived from atomic targets, the same conclusions should hold for molecules too (where “exact” calculations are not possible). For molecules, the results have important implications. Both elastic scattering and photoionization are the standard methods for studying the structure of atoms and molecules in conventional energy domain measurements, thus high-energy photoelectrons and high harmonics generated by infrared lasers offer the promise for revealing the structure of the target, with the temporal resolution offered by the ultrashort laser pulses.

Consider a typical few-cycle laser pulse, with mean wavelength of 800 nm and peak intensity of 10^{14} W/cm². The electric field $\mathbf{F}(t) = -\partial\mathbf{A}(t)/\partial t$ and the vector potential $\mathbf{A}(t)$ of such a laser pulse are depicted in Fig. 1(a). By placing a hydrogen atom in such a laser pulse, we solved the TDSE to obtain the photoelectron energy and momentum distributions, shown in Figs. 1(b) and 1(c), respectively. Fig. 1(d) shows the electron momentum image of Ar in the same laser pulse. The theoretical method for solving the TDSE has been described previously [11].

In Fig. 1(b), two particular energies, $2U_p$ and $10U_p$, are marked, where $U_p = A_0^2/4$ is the ponderomotive energy, with A_0 being the peak value of the vector potential of the laser pulse. (We use atomic units in this paper.) These two energy values are important, the former is the maximum energy the electron can reach if it is released by the laser field alone, while the latter is the maximum

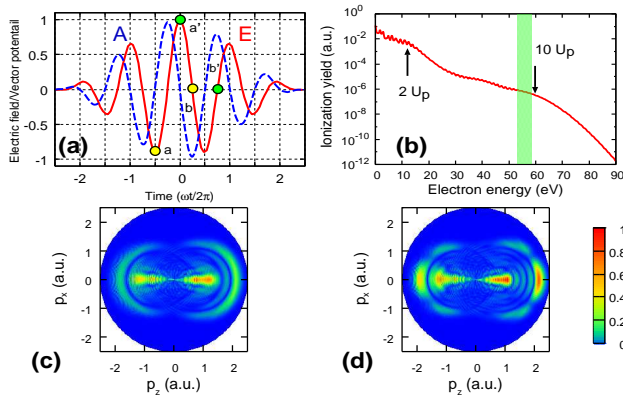


FIG. 1: (Color online) (a) Schematic of the electric field (E) and the vector potential (A) of a typical few-cycle pulse. (b) Energy spectra of atomic hydrogen ionized by a 5 fs (FWHM) laser pulse, with mean wavelength of 800 nm and peak intensity at 10^{14} W/cm 2 . (c) Normalized 2D photoelectron momentum spectra of atomic hydrogen. The images are renormalized for each photoelectron energy to reveal the global angular distributions. (d). Momentum images of Ar in the same pulse.

energy the electron will have if it is back scattered by the parent ion [12]. To display the full electron momentum image surface in a single plot, in Figs. 1(c) and 1(d) we normalized electron momentum distributions such that the total ionization yield at each electron energy is the same. We have chosen the horizontal axis to be along the direction of the laser’s polarization and the vertical axis along any direction perpendicular to it (due to cylindrical symmetry of the linearly polarized light).

In Figs. 1(c) and 1(d), we note that in the large momentum region, each image exhibits two half circular rings, one on the “left” and one on the “right”, with the center of each circle shifted from the origin. The rings are very similar for the two targets. We will call these circular rings back rescattered ridges (BRR), representing electrons that have been rescattered into the backward directions by the target ion. The BRR on the “right” is from electrons born at time near ‘a’ (Fig. 1(a)), traveling to the “right” and then returning to the target ion at time near ‘b’, where they are rescattered back to the right. Each momentum half circle is represented approximately by $A_r \hat{p}_z + p_0 \hat{p}_r$, where the second term is the momentum of the backscattered electron and the first term is the momentum added to the electron as it propagates from ‘b’ to the end of the laser pulse. The magnitude of the momentum p_0 is related to the ponderomotive energy by $3.17 \bar{U}_p = p_0^2/2$ (where $\bar{U}_p = A_r^2/4$, and A_r is the vector potential at ‘b’), which is the maximum energy of electrons that return to revisit the parent ion. For back scattered electrons, the two momentum terms add to give high-energy photoelectrons, reaching a maximum of $10U_p$ for electrons that have been scattered by 180° [12]. If the

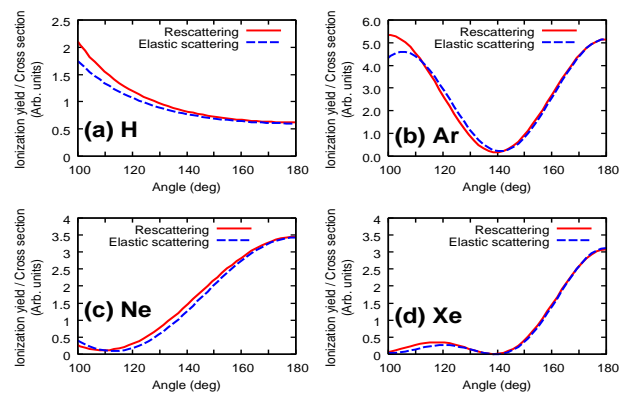


FIG. 2: (Color online) Angular distributions of photoelectrons along the BRR compared to the differential elastic scattering cross sections of the target ion. Each BRR is taken to be the outer half circle on the right side of Fig. 1(c) and 1(d), respectively. (a) for H target. (b) for Ar, (c) for Ne, (d) for Xe.

electrons are scattered into the forward direction, the two momentum terms subtract from each other, resulting in lower energy electrons. Similar back scattered electrons are found on the “left”. These are from electrons that were born near ‘a’ and rescattered back to the left near ‘b’ [Fig.1(a)]. Both the shift of the center and the radius are smaller due to rescattering occurring in the smaller vector potential near ‘b’.

In Figs. 1(c) and 1(d), we note that the yields on the BRR for H and Ar are quite different, where the former is monotonic and the latter has a clear minimum. Taking the actually calculated photoelectron yields (without the normalization as shown in the figure) we compare the angular dependence of the intensities along BRR with the elastic differential cross sections of the target ion by *free* electrons at energy $E = p_0^2/2$. The results are shown in Fig. 2(a) for H target and 2(b) for Ar, where the scattering angles are measured from the direction of the “incident” electron beam. Good agreement between the two results for each target atom can be seen. Such good agreement has been duplicated at different laser intensities and other atomic systems [see Ne and Xe in Figs. 2(c) and 2(d), respectively.]. These results show that laser-induced momentum images on the BRR can be used to obtain elastic scattering cross sections of free electrons by the target ion. For atomic hydrogen, the elastic scattering cross section is given by the Rutherford formula. For other atomic ions, minima in the differential cross section do occur and they are due to interference between electrons scattered by the short-range potential and by the Coulomb potential [13]. We comment that momentum spectra due to back scattered electrons have been observed experimentally earlier [14] but there has been no quantitative analysis.

According to the intuitive rescattering model, the photoelectron yield along the BRR may be interpreted as due

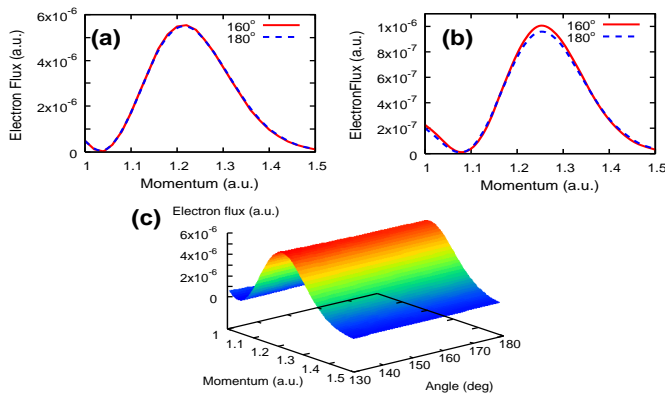


FIG. 3: (Color online) Electron wave packets extracted from photoelectron momentum images along the BRR are shown to be identical for scattering angles of 160° and 180° , extracted from (a) H target, (b) Ar target, using the same ionizing laser. (c) The extracted electron wave packet from H target is the same over the angular range of 130° to 180° .

to back scattering of the returning electron wave packet. To test this idea, we write the photoelectron momentum yields $I(\mathbf{p})$ along the BRR by $I(\mathbf{p}) = \sigma(p_0, \theta)F(p_0, \theta)$, with $\mathbf{p} = A_r \hat{\mathbf{p}}_z + p_0 \hat{\mathbf{p}}_r$, where $\sigma(p_0, \theta)$ is the elastic differential cross section for each ion by a free electron with energy $E = p_0^2/2$, and θ is the scattering angle of the free electron.

In Fig. 3(a), we show that the extracted $F(p_0, \theta)$ from H at two different angles. They are essentially identical such that we may identify $F(p_0) = F(p_0, \theta)$ as the wave packet of the returning electrons with momentum near p_0 . Note that the wave packet extracted from Ar target, as shown in Fig. 3(b), is essentially identical to Fig. 3(a) except for a small shift of the center from $p_0 = 1.22$ to 1.25. The width of the wave packet is found to be independent of the target. In Fig. 3(c) we show that $F(p_0) = F(p_0, \theta)$ indeed holds well for electrons that have been back scattered for angles larger than about 130° . Note that a separate electron wave packet can be retrieved from the photoelectron momentum spectra measured on the “left”. The wave packet analyzed above is for a 5 fs (FWHM) pulse with the carrier-envelope phase (CEP) $\phi = 0$. The returning electron wave packet depends on the CEP and can be used to measure the CEP of a few-cycle pulse. For long pulses, electrons along each side of the BRR will exhibit oscillations characteristic of ATI peaks, and elastic scattering cross sections by free electrons can be extracted from the envelope of the momentum images on the BRR [15].

The above results, based on the exact solution of TDSE, clearly established that the electron yields on the BRR, can be viewed as the backscattering of the returning electron wave packet. According to the “simple man” model, the HHG is due to the emission of photons following the photo-recombination of the same returning elec-

trons. Since the returning electron wave packets have been shown largely independent of target atoms for the same laser pulse, the difference in the HHG spectra would then be attributed to the recombination cross sections. To check this idea, we choose a companion atom to have the same ionization potential I_p such that the cutoff energies will be identical. In the calculation, we compare the HHG spectra for Ne and scaled model hydrogen atom, generated by the same laser field, by solving the TDSE. For Ne atom, it is ionized from the $2p_0$ state, and for H, we chose an effective charge such that its ground $1s$ state has the same ionization potential as Ne. For the laser, we chose a 5.2 fs pulse, with mean wavelength of 1064 nm and intensity of 2×10^{14} W/cm². The longer wavelength was used such that harmonics would extend over a larger photon energy range. From the calculated HHG yield, we divide each by its “exact” photo-recombination cross section. We compare in Fig. 4(a) the resulting “electron wave packets” (normalized) vs the HHG order. Clearly the two electron wave packets are very close to each other, showing that the differences in the HHG spectra between the two targets are coming from the different photo-recombination cross sections. Note that the kinetic energy of the photoelectron is related to the photon energy by $\hbar\omega = k^2/2 + I_p$. Also note that the deduced “electron wave packet” shows many oscillations. To study the structural information of a target, it is much easier to factor out these oscillatory features by using a known companion atomic target.

The good agreement in the deduced “electron wave packet” in Fig. 4(a) prompts us to ask whether one can obtain accurate photo-recombination cross sections from the HHG spectra of an unknown target by comparing it with the HHG spectra from a known atom with identical or nearly identical ionization potential. For our purpose we generated the HHG spectra for Ar and scaled H atoms, with the effective charge of H chosen to have identical ionization potential as Ar. Different laser intensities and wavelengths were used to generate HHG from which Ar recombination cross sections are derived. If the procedure is valid, the extracted recombination cross sections should be independent of the lasers used, except for the range of photon energies covered. In Fig. 4(b) we compare the extracted cross sections from the HHG generated by various laser pulses with the “exact” photo-recombination cross section calculated for Ar. One can see that the deduced values scatter nicely around the “exact” one. The fluctuation of the extracted cross sections can be reduced if the HHG intensity is taken from the averaged HHG *amplitudes* with nearby laser intensities. Thus the smooth black line is obtained from averaging over eleven intensities within $\pm 5\%$ of the mean intensity of 2×10^{14} W/cm². This coherent averaging sharpens the odd harmonics and reduces the harmonic yields in between, similar to the effect of propagation of HHG in the medium. Note that in the “exact” calculation we include

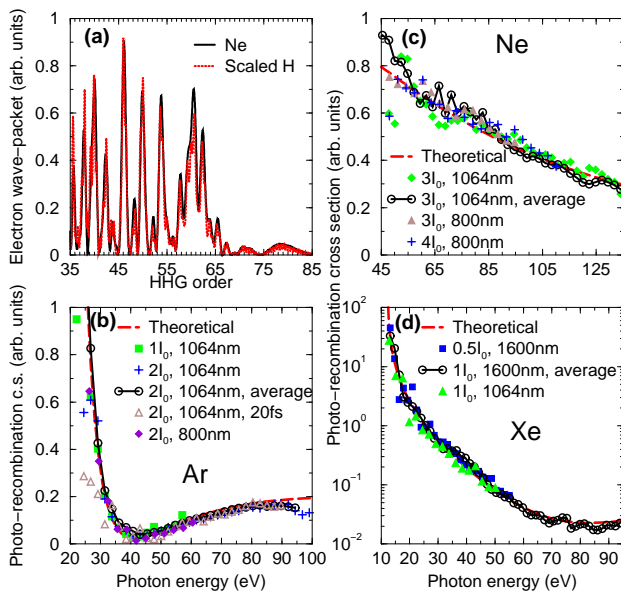


FIG. 4: (Color online) (a) Comparison of the “electron wavepackets” extracted from the HHG spectra of Ne and scaled H generated by a 5.2 fs laser pulse with peak intensity of 2×10^{14} W/cm² and mean wavelength of 1064 nm. Extracted photo-recombination cross sections of Ar (b), Ne (c) and Xe (d), using different laser pulses, plotted vs the photon energy. For each panel, the dashed red line is the “exact” theoretical cross section, calculated using the same model potential, as used in the TDSE. ($I_0 = 10^{14}$ W/cm².)

dipole transitions from 3p to both s and d continuum states. The minimum in the cross section occurs near the Cooper minimum where the d-wave electric dipole moment changes sign. Comparing the two curves we can say that accurate photo-recombination cross sections indeed can be extracted from the HHG yields. Similar test showing good agreement has been made also on Ne and Xe atoms (Figs. 4(c) and 4(d)), again using scaled hydrogen as the companion atoms.

Following last paragraph, we now comment the assumptions made in Itatani *et al* [7]. Their assumption that the returning electron wave packets for Ar and N₂ (they have nearly identical ionization potentials) are the same under the same laser pulse is confirmed by our calculations which are based on exact solution of the TDSE. However, it was also assumed [7, 10] that the dipole matrix elements can be calculated using plane waves instead of “exact” scattering waves. This leads to results that are quite different from ours.

In this Letter we have identified the spectral region where the *nonlinear* laser-atom interaction can be simplified to extract the *linear* interaction between a returning electron wave packet with the atomic ion. Even though the results were presented for atomic targets, the same

simplifications should hold for molecular targets as well. For molecules, this opens up the exciting opportunity of using infrared lasers for ultrafast imaging of molecules undergoing structural transformation. Both elastic electron scattering and photoionization (the inverse of photo-recombination) processes are the well-tested means for probing the structure of molecules. They depend linearly on the electron current and photon intensity, respectively. Theoretically, these cross sections can be calculated very precisely. A computer package for obtaining elastic scattering cross section and photoionization cross section within such a model has been published recently by Tonzani [16]. By extracting elastic and/or photo-recombination cross sections of molecules using few-cycle infrared lasers, structural changes of the molecules can be determined with temporal resolution of a few femtoseconds. In conclusion, we have established the theoretical foundation for carrying out structural analysis of molecules with infrared lasers. If this roadmap is implemented experimentally, table-top infrared lasers would offer a very competitive new technology for ultrafast time-resolved chemical imaging, with temporal resolution down to a few femtoseconds.

This work was supported in part by the Chemical Sciences, Geosciences and Biosciences Division, Office of Basic Energy Sciences, Office of Science, U. S. Department of Energy. TM is supported by a Grant-in-Aid for Scientific Research (C) from the Ministry of Education, Culture, Sports, Science and Technology, Japan, by the 21st Century COE program on “Coherent Optical Science”.

-
- [1] A. Zewail, *Annu. Rev. Phys. Chem.* **57**, 65 (2006).
 - [2] T. Zuo *et al.*, *Chem. Phys. Lett.* **259**, 313 (1996).
 - [3] M. Spanner *et al.*, *J. Phys. B: At. Mol. Opt. Phys.* **37**, L243 (2004).
 - [4] S. X. Hu, L. A. Collins, *Phys. Rev. Lett.* **94**, 073004 (2005).
 - [5] M. Lein *et al.*, *Phys. Rev. A* **66**, 051404(R) (2002).
 - [6] S. N. Yurchenko *et al.*, *Phys. Rev. Lett.* **93**, 223003 (2004).
 - [7] J. Itatani *et al.*, *Nature* **432**, 867 (2004).
 - [8] V. H. Le *et al.*, *Phys. Rev. A* **76**, 013414 (2007).
 - [9] S. Patchkovskii *et al.*, *Phys. Rev. Lett.* **97**, 123003 (2006).
 - [10] J. Levesque *et al.*, *Phys. Rev. Lett.* **98**, 183903 (2007).
 - [11] Z. Chen *et al.*, *Phys. Rev. A* **74**, 053405 (2006).
 - [12] G. G. Paulus *et al.*, *J. Phys. B: At. Mol. Opt. Phys.* **27**, L703 (1994).
 - [13] A. Messiah, *Quantum Mechanics*. Vol. I, p. 428, (North-Holland Publishing, Amsterdam, 1958).
 - [14] B. Yang *et al.*, *Phys. Rev. Lett.* **71**, 3770 (1993).
 - [15] Z. Chen *et al.*, *Phys. Rev. A* (submitted).
 - [16] S. Tonzani, *Comput. Phys. Comm.* **176**, 146-156 (2007).